5 Supplementary material

5.1 Conductance of membrane proteins

The (electrical charge) currents entering Eq. 1 and Eq. 4 are themselves dynamic quantities. Channels are gated in dependence on the membrane potential, on the presence of ATP, and on glucose- and ion- concentration. The resulting current depends on the electrochemical gradient over the membrane. So every membrane protein has its own characteristics and the conductance of passive or active ion flow depends on different other parameters. In the following the different membrane proteins (as listed in Tab. 1) and their gating/activity properties are described in more

Na,K	sodium-potassium exchanger (Na^+ outwards, K^+ inwards)
Na,V	voltage-gated sodium channels
NCX	sodium-calcium exchanger (Na^+ inwards, Ca^{2+} outwards)
PMCA	Plasma-membrane-calcium-ATPase (Ca^{2+} outwards)
K,ATP	ATP-driven (and glucose-dependent) potassium channels
K,V	voltage-gated potassium channels (also called delayed rectifier)
sK,Ca	small conductance calcium-gated potassium channel
K,Ca	large conductance voltage- and calcium-gated potassium channel
Ca,L	L-type voltage-dependent calcium channels
Ca,T	T-type voltage-dependent calcium channels

Table 1: **Acronyms of transmembrane proteins:** Acronyms for the different plasma membrane proteins contributing to ion flow through the membrane are defined. *Inwards* and *outwards* specifies in which direction the ion flows, i.e. in or out of the cell.

detail. Currents through pores are generally approximated by a linear voltage-current relation, which infers currents proportional to the electrical potential gradient (terms with $V - \overline{V}$ with $\overline{V}$ the reversal potential of the ion under consideration). For some channels and for extreme depolarisations there might be deviations from this approximation.

The activation dynamics of active carrier proteins relies on the Hill-function

$$H(x, x_h, n) = \frac{x^n}{x^n + x_h^n} \quad , \tag{6}$$

which can be derived from chemical kinetics. x denotes some concentration, x_h is the corresponding concentration of half activation, and n is the Hill-coefficient. Large n make the switch between inactive and active states steeper.

The asymptotic state of activation and inactivation is described by two functions of sigmoidal shape

$$\begin{aligned} \sigma_{\mathrm{act}}(x, x_{\mathrm{h}}, \kappa) &= \frac{1}{1 + \exp\{(x_{\mathrm{h}} - x)/\kappa\}} \\ \sigma_{\mathrm{inact}}(x, x_{\mathrm{h}}, \lambda) &= \frac{1}{1 + \exp\{(x - x_{\mathrm{h}})/\lambda\}} \quad , \end{aligned} \tag{7}$$

Such sigmoidal functions are frequently used in literature and the parameters of these functions are determined in experiments. x_h is the concentration of half-maximum value and κ and λ regulate the activation and inactivation steepness, respectively. Inactivation is a property of ion channels which will be handled in complete analogy to activation. In a first approximation ATPases driving ions against their chemical gradient are inactivated. Only the channels Na,V; K,V; K,Ca; Ca,L; and Ca,T (see Tab. 3 and 4) are subject to inactivation.

5.1.1 The sodium-potassium exchanger Na,K

The sodium potassium exchanger transports sodium out of the cell and potassium into the cell. Both transport processes are against the chemical gradient, so that this process has to consume energy which is provided by ATP. The current is modelled as

$$I_{\mathrm{Na,K}} \;=\; \overline{I_{\mathrm{Na,K}}}\,(1 - H(K, K_{\mathrm{Na,K}}, n_{\mathrm{Na,K}}))\, H(N, \tilde{K}_{\mathrm{Na,K}}, \tilde{n}_{\mathrm{Na,K}}) \quad , \tag{8}$$

where $\overline{I_{\mathrm{Na,K}}}$ denotes the maximum current. The quantities used for the Hill-function are explained after Eq. 6. The first term describes a decreasing activity with increasing potassium concentration. The second one an increasing activity with increasing sodium concentration (see (49)). This approach follows approximations frequently adopted in other models: The adaption of Na,K-activity to sodium and potassium levels is assumed quick such that the steady state approximation is justified. A direct impact of glucose on Na,K-activity in β-cells (50) and a voltage-dependence of Na,K-activity (49) is neglected. As ATP-dynamics are not modelled, the ATP-level does not influence Na,K-activity.

Activation dynamics: The used parameters follow those found in (49) to fit experimental activation dynamics. Good agreement is found with $n_{\mathrm{Na,K}} = 2$ and $K_{\mathrm{Na,K}} = 33mM$ as well as $\tilde{n}_{\mathrm{Na,K}} = 2$ and $\tilde{K}_{\mathrm{Na,K}} = 20mM$ for dependence on potassium and sodium, respectively.

Stoichiometry: The stoichiometry of the exchanger is 3:2, thus 3 sodium ions are exchanged against 2 potassium ions entering the cell, i.e. $\alpha_{\mathrm{Na,K}} = 1.5$ in Eqs. 1 and 4. As both ions have the valence 1 this corresponds to 1 positive charges leaving the cell for 2 potassium ions entering the cell. Thus $\overline{I_{\mathrm{Na,K}}} > 0$ enters the different equation with different factors: $+1$ for V Eq. 4, -2 for K, and $+3$ for N Eq. 1.

Turnover rate: The turn over rate of one ATPase measured as the consumption of ATP-molecules per second is $\overline{I_{\mathrm{Na,K}}} = 200ATP/sec \approx 0.00003pA$ in canine cardiac neurons (51), where the last equality assumes one exchange of 3 sodium and 2 potassium per ATP.

5.1.2 The voltage gated sodium channel Na,V

The voltage gated sodium channel opens when the cell is depolarised. The sodium ions then follow their electrochemical gradient to flow into the cell. The current is therefore composed of two factors, one describing the open-probability of the channel, the other describing the flow through the open channel:

$$I_{\mathrm{Na,V}} \;=\; h_{\mathrm{Na,V}} g_{\mathrm{Na,V}} \overline{g_{\mathrm{Na,V}}} \left(V - \overline{V_{\mathrm{Na}}}\right) \quad . \tag{9}$$

$\overline{V_{\mathrm{Na}}}$ is the sodium reversal potential, and $\overline{g_{\mathrm{Na,V}}}$ is the maximum conductance. The open and inactivation probabilities $g, h_{\mathrm{Na,V}}$ are assumed to exponentially reach their asymptotic values and, thus, follow the kinetic equations

$$\begin{aligned} \frac{dg_{\mathrm{Na,V}}}{dt} &= \frac{\sigma_{\mathrm{act}}(V, V_{\mathrm{Na,V}}, \kappa_{\mathrm{Na,V}}) - g_{\mathrm{Na,V}}}{\tau_{\mathrm{Na,V}}} \\ \frac{dh_{\mathrm{Na,V}}}{dt} &= \frac{\sigma_{\mathrm{inact}}(V, W_{\mathrm{Na,V}}, \lambda_{\mathrm{Na,V}}) - h_{\mathrm{Na,V}}}{\theta_{\mathrm{Na,V}}} \quad . \end{aligned} \tag{10}$$

The parameters are explained after Eq. 7. It is $\tau_{\mathrm{Na,V}}$ that defines the time constant of adaptation of the sodium channel (the speed of conformity change) in response to a changed membrane potential, while $\theta_{\mathrm{Na,V}}$ determines the time scale of channel inactivation.

Conductance: The single channel conductance of the voltage-gated sodium channel is $\overline{g_{\mathrm{Na,V}}} = 14pS$ as found in the squid axon (52). This value is consistent with findings in other systems. Taking the results in mice β-cells (19), one has a single channel current of $1pA$ at $-30mV$ which (using $V_{\mathrm{Na}} = 80mV$) corresponds to $9pS$.

Activation properties: Activation is observed between $-60mV$ and $-10mV$ (19). Thus, a realistic approximation for the activation dynamics is $V_{\mathrm{Na,V}} \approx -35mV$ and $\kappa_{\mathrm{Na,V}} \approx 8mV$.

Inactivation properties: The role of voltage-gated sodium channels in insulin secretion and in membrane depolarisation is controversial. Depending on species, the half-maximal inactivation is found at $-109mV$ in mouse β-cells (19) (where $2.6mM$ calcium were used, and at less calcium the inactivation point was shifted to even lower voltage) and total inactivation is found at $-40mV$ (27, 33). Thus, one may estimate $W_{\mathrm{Na,V}} \approx -100mV$ with a steepness of $\lambda_{\mathrm{Na,V}} \approx 20mV$ (in order to get the observed total suppression of inactivation at $-150mV$, and total inactivation at $-40mV$). This very low half inactivation potential if fully consistent with measurement in islet-β-cells (26) and suggests an unprobable major role in the electrophysiology of β-cells (19), which is not confirmed in the present simulations.

Time scales: According to the sodium currents as observed in squid giant axons and to the classical description by Hodgkin-Huxley the time constant of activation depends on the membrane potential (15). This is represented by

$$\tau_{\mathrm{Na,V}} = \frac{c}{\exp\{(V - V_0)/a\} + \exp\{(V_0 - V)/b\}} \tag{11}$$

with $c = 11.5ms$, $a = 40mV$, $b = 50mV$, and $V_0 = -70mV$. Similar $\tau_{\mathrm{Na,V}}$ are found in islet-β-cells (26). Note that the same simulation results are found with the constant average value of $\tau_{\mathrm{Na,V}} = 3ms$. Inactivation happens on a time scale of $\theta_{\mathrm{Na,V}} = 4.6ms$ which was found by two pulse experiments (15).

Calcium permeability of sodium channels: Sodium channels in neurons are in general permeable for calcium ions. Therefore, Na,V-channels are explicitly blocked with TTX in experiments to investigate the opening dynamics of voltage-gated calcium channels in order to separate these from the currents through sodium channels (see e.g. (18)). Calcium permeability of Na,V is not considered in the present approach.

5.1.3 The sodium-calcium exchanger NCX

The sodium-calcium exchanger takes advantage of the electrochemical gradient of sodium (pushing sodium into the cell) to transport calcium ions against its electrochemical gradient. This exchanger is important to reestablish the resting state calcium concentration after an excitable calcium influx into the cell. As in the case of the sodium-potassium exchanger a fast adaption of the activity to the calcium concentration is assumed. The current is derived from a corresponding Hill-function:

$$I_{\mathrm{NCX}} \quad = \quad \overline{I_{\mathrm{NCX}}} H(C, C_{\mathrm{NCX}}, n_{\mathrm{NCX}}) \quad . \tag{12}$$

Typical values for the single membrane protein parameters can be found in (12): $\overline{I_{\mathrm{NCX}}} = -0.0005pA$ (53) and $C_{\mathrm{NCX}} = 0.0022mM$ (10). The Hill coefficient is assumed to be $n_{\mathrm{NCX}} = 1$. This is justified by the linear relationship between the observed current and the calcium concentration as observed for low calcium concentrations in cardiac cells (54). However, the NCX-Hill-coefficient is controversial (2, 11).

Stoichiometry: The stoichiometry of NCX is 3:1, i.e. $\alpha_{\mathrm{NCX}} = 3$ in most tissues (10), thus three sodium ions have to enter the cell in order to expel one calcium ion. The net current of NCX is one positive charge getting into the cell for every expelled calcium ion. This infers that $\overline{I_{\mathrm{NCX}}} < 0$. I_{NCX} enters the different equations with factor $+1$ for the equation for the membrane potential Eq. 4, a factor -1 in the calcium equation, and a factor α_{NCX} in the sodium equation Eq. 1.

Impact of sodium-concentration: Note that in the present description Eq. 12 the sodium concentration does not enter, even though NCX activity also depends on the sodium concentration gradient (11). Even though the sodium dynamics is modelled, it is assumed that the sodium concentration gradient is approximately constant. This turns out to be a reasonable approximation. In contrast, to neurons, in β-cells peaks in the potential are dominantly generated by calcium and not by sodium.

Impact of ATP: A dependence of the NCX activity on intracellular ATP concentration has been observed (55). This might be included in improved versions of this model that treat ATP dynamically.

5.1.4 PMCA

PMCA is an ATP-driven calcium pump extruding calcium from the cell to the extracellular medium, which has been characterised in β-cells (56). In a first attempt the dependence on the ATP concentration is ignored and the ATP-concentration is assumed to be large enough to make the pump work optimally. Then the activity is mainly dependent on the calcium concentration in the cell. A suitable modelling approach is (see also (2))

$$I_{\mathrm{PMCA}} \quad = \quad \overline{I_{\mathrm{PMCA}}} H(C, C_{\mathrm{PMCA}}, n_{\mathrm{PMCA}}) \quad . \tag{13}$$

The maximum current $\overline{I_{\mathrm{PMCA}}}$ is positive, as it carries calcium out of the cell. A delayed activation of PMCA by increased calcium has been observed (57) which is neglected in the present

model (using the steady state approximation).

Stoichiometry: One calcium ion is transported per used ATP molecule leading to the stoichiometry of $\alpha_{\mathrm{PMCA}} = 1$ (58). This is surprising in view of the Hill-coefficient which was determined to be $n_{\mathrm{PMCA}} = 2$ (59), which would suggest a corresponding stoichiometry (see also the discussion in (60)).

Turnover rate: The turnover rate of single PMCA is in the order of 30 Hertz (53) corresponding to an activity rate of $k_a = 0.03/ms$ (this value was also used in (3)). This turnover rate can be translated into an electrical current: Every pumping event corresponds to a flow of 2 electrical charges e leading to $\overline{I_{\mathrm{PMCA}}} = z_{\mathrm{Ca}} e k_a = 60 \cdot 1.6 \cdot 10^{-19} C/s \approx 10^{-17} A = 10^{-5} pA$.

Half activation concentration: Typical values for the half activation calcium concentration are $C_{\mathrm{PMCA}} = 0.1 \mu M$ (see e.g. (61) Figure 3). Note that the values of half activation are found to depend on the calmodulin concentration and the isoform under consideration (61) which is neglected in the present approach. The 4b-isoform has a slightly larger half activation concentration of $0.16 \mu M$ (61).

ATP consumption: If modelling ATP concentration dynamics PMCA has to be considered as a major consumer of ATP. Note that up to 40% of the ATP consumed to pump calcium out of the cell is used by SERCA-ATPase, thus, not in the plasma membrane but at the endoplasmatic reticulum (22).

5.1.5 ATP-driven potassium channel K,ATP

The ATP-driven potassium-selective channel (also called G-channel (8)) uses ATP to open the channel and to release potassium from the cell. This process is, however, also regulated by the presence of glucose which is a source for ATP-metabolism in mitochondria. At normal glucose levels the channel has a resting state open probability, which is counteracted by the activity of the sodium-potassium exchanger. Note that about 50% of the potassium current is mediated by K,ATP channels (7). At increased levels of glucose the opening of this channel is inhibited. The single protein current is modeled by (see also Eq. 9):

$$I_{\mathrm{K,ATP}} = (1 - g_{\mathrm{K,ATP}}) \overline{g_{\mathrm{K,ATP}}} \left(V - \overline{V_{\mathrm{K}}}\right) \quad , \tag{14}$$

with

$$\frac{dg_{\mathrm{K,ATP}}}{dt} = \frac{\sigma_{\mathrm{act}}(\gamma, \gamma_{\mathrm{K,ATP}}, \kappa_{\mathrm{K,ATP}}) - g_{\mathrm{K,ATP}}}{\tau_{\mathrm{K,ATP}}} \quad . \tag{15}$$

Here, γ is the glucose concentration. All other parameters are in full analogy to the voltage-gated sodium channel Na,V.

Ohmic conductance and calcium dependence: In the resting state the current dominantly flows through this channel (27) which explains why the resting potential is near of the potassium reversal potential. It is controversial whether the current-voltage relation is ohmic ((27) versus (8, 9, 26)). The latter authors show an ohmic relation in the relevant range of membrane potentials which justifies the present model (see (9) Fig. 2, (8) Fig. 1b). The opening frequency

is observed to depend neither on the membrane potential nor on the calcium level (9, 26, 27) which justifies the present approximation Eqs. 14 and 15.

Conductance: The conductance of single open channels is in the order of $50pS$ for relevant membrane potentials (8) where also the dependence on the glucose level was investigated. This is consistent with the finding that with increasing depolarisation of the cell increasing outflow of potassium is observed with a single channel conductance of $\overline{g_{\mathrm{K,ATP}}} = 54pS$ (9) (this value is used throughout all present simulations). An approximately linear current-voltage-relationship is found (9).

Activation time scale: The steady state approximation was used in two other models (4, 5). This points to a relatively short $\tau_{\mathrm{K,ATP}}$. However, in an effective modelling approach (ignoring ATP concentrations) the time constant does not represent the time needed for the channel to adapt to a novel ATP-concentration but the time needed for the full metabolism process from glucose through ATP generation up to the changed open probability. The whole process from increased glucose levels up to exocytosis of insulin carrying granules take 1 minute (62), which defines an upper limit for $\tau_{\mathrm{K,ATP}}$. Thus, $\tau_{\mathrm{K,ATP}}$ is chosen between this time and the time scale

Glucose-driven deactivation: As K,ATP provides the dominant part of potassium current in resting state it is assumed that the half-deactivation-concentration of K,ATP is around the resting level of glucose ($\gamma_{\mathrm{K,ATP}} = 1.2mM$). The steepness of the dependence on glucose is estimated as $\kappa_{\mathrm{K,ATP}} = 6mM$.

Modelling ATP-dynamics: The present simulation might be improved by inclusion of ATP-dynamics as done in (2, 6). The functional relationship is well supported by experiment (21). This will be subject of further research.

Other ATP-driven potassium channels Other, novel, ATP-activated potassium channels have been observed in mice and humans, however, they differ in characteristics. They are still poorly defined but they are also believed to be involved in calcium oscillations. One additional channel found in human β-cells has a single-channel potassium conductance of $30pS$ (27).

5.1.6 The voltage-gated potassium channel K,V

The voltage gated potassium channel (also called delayed rectifier potassium channel) increases the potassium efflux from the cell once the cell is depolarised. The potassium ions follow their electrochemical gradient. The model for this channel is in complete analogy to the voltage-gated sodium channel Eq. 9:

$$I_{\mathrm{K,V}} = h_{\mathrm{K,V}} g_{\mathrm{K,V}} \overline{g_{\mathrm{K,V}}} \left(V - \overline{V_{\mathrm{K}}}\right) \quad , \tag{16}$$

with

$$\begin{aligned} \frac{dg_{\mathrm{K,V}}}{dt} &= \frac{\sigma_{\mathrm{act}}(V, V_{\mathrm{K,V}}, \kappa_{\mathrm{K,V}}) - g_{\mathrm{K,V}}}{\tau_{\mathrm{K,V}}} \\ \frac{dh_{\mathrm{K,V}}}{dt} &= \frac{\sigma_{\mathrm{inact}}(V, W_{\mathrm{K,V}}, \lambda_{\mathrm{K,V}}) - h_{\mathrm{K,V}}}{\theta_{\mathrm{K,V}}} \quad . \end{aligned} \tag{17}$$

This is largely analogous to other models of β-cell bursting (2, 4, 5). However, the activation characteristics are not consistent in these models and inactivation is not considered ((4) includes a different inactivating channel called $I_{\rm fast}$ therein). The present model is based on single protein properties exclusively derived from experiment.

Conductance: Open channels have a single channel conductance of $\overline{g_{\rm K,V}} = 10pS$ (27).

Voltage-dependent activation: K,V-channels in human β-cells were activated with a $400ms$ depolarisations to different membrane potentials (29). Then the membrane potential was reduced to -50mV and the current after this reset was monitored. The authors find a sigmoidal shape, centered at $V_{\rm K,V} = 1mV$ and width $\kappa_{\rm K,V} = 8.5mV$.

Time scale of activation: The activation time constant is assumed to depend on the potential in (3) according to

$$\tau_{\rm K,V} \quad = \quad \frac{c}{\exp\{(V - \overline{V_{\rm K}})/a\} + \exp\{-(V - \overline{V_{\rm K}})/b\}} \tag{18}$$

with $c = 60ms$, $\overline{V_{\rm K}} = -75mV$, $a = 65mV$, and $b = 20mV$. This function is in agreement with experiments where the time constant was found to vary between 8 and $37ms$ (29).

Slow channel inactivation: For long depolarisations inactivation of the channels is observed. The characteristics are $W_{\rm K,V} = -25mV$ and width $\lambda_{\rm K,V} = 7.3mV$ (29). However, inactivation is not observed within $400ms$ so that we must conclude that $\theta_{\rm K,V} > 400ms$. The value of $400ms$ is used in all simulations.

5.1.7 Calcium-gated potassium channel K,Ca

There are two-types of calcium-gated potassium channel. Both open in dependence of intracellular calcium levels. However, the conductance, the range of calcium concentrations optimal for channel opening, and the dependence on the membrane potential differ strongly.

This section describes the large conductance calcium-gated potassium channel which also exhibits a dependence on the membrane potential. The dependence of the open probability on calcium is assumed to be in steady state and described by a Hill-function. Voltage-gating is described by on Ohm-like approach with dynamic gating (see also Eq. 9).

$$I_{\rm K,Ca} \quad = \quad g_{\rm K,Ca}\overline{g_{\rm K,Ca}} \left(V - \overline{V_{\rm K}}\right) H(C, C_{\rm K,Ca}, n_{\rm K,Ca}) \quad , \tag{19}$$

with

$$\frac{dg_{\rm K,Ca}}{dt} \quad = \quad \frac{\sigma_{\rm act}(V, V_{\rm K,Ca}, \kappa_{\rm K,Ca}) - g_{\rm K,Ca}}{\tau_{\rm K,Ca}} \tag{20}$$

All parameters are in analogy to other proteins described before. The models (2,4,5) differ from the present one by very large Hill-coefficients (between 3 and 5) in a single Hill-function. A very detailed model of K,Ca-dynamics was developed before (36). Here a more phenomenological approach to single K,Ca-channel characteristics is followed.

Ohmic conductance: The calcium-gated potassium channel is rapidly activated upon depolar-

isation and show a linear current-voltage relation (27). This justifies usage of an Ohm's law current.

Conductance: The conductance of single-channels $\overline{g_{\mathrm{K,Ca}}} = 220pS$ is rather large (27). This is also confirmed in rat muscle cells with values of up to $300pS$ depending on the temperature (14).

Opening dynamics: Experiments with rat muscle cells (14) show a dynamic activation in dependence on the membrane potential and of the calcium concentration (see also (27)). A sigmoidal opening probability is found for constant membrane potential in dependence of different calcium concentrations (see (14) Fig. 6), but also for constant calcium with variable membrane potential (see (14) Fig. 8).

In a first approximation the opening dynamics is modelled by a product of a sigmoidal function and a Hill-function as shown in Eqs. 19 and 20. However, this approach turns out to be in contradiction to the data in (14). In order to reproduce these measurements more accurately, a dependence of the half activation calcium concentration $C_{\mathrm{K,Ca}}(V)$ on the voltage has to be assumed (see Figure 12):

$$\begin{aligned} \frac{dC_{\mathrm{K,Ca}}}{dt} &= \frac{C^{\infty}_{\mathrm{K,Ca}}(V) - C_{\mathrm{K,Ca}}}{\tau_{\mathrm{K,Ca}}} \quad , \\ \text{with} \qquad C^{\infty}_{\mathrm{K,Ca}}(V) &= \exp\left\{\frac{a-V}{b}\right\} \end{aligned} \tag{21}$$

with $a = 45mV$ and $b = 30mV$, and the same time delay than for the direct voltage-dependence (assuming related mechanisms). This is combined with a Hill-coefficient of $n_{\mathrm{K,Ca}} = 2$ and the

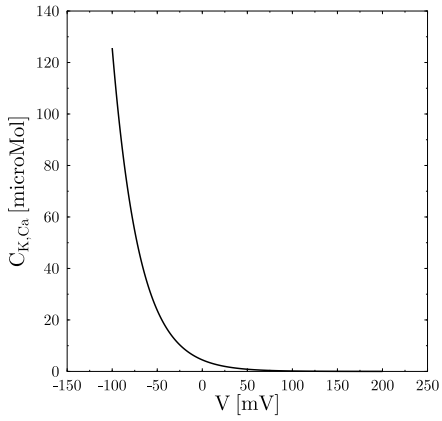

Figure 12: **Voltage-dependence of half activation:** The steady-state voltage-dynamics of the half activation calcium concentration $C^{\infty}_{\mathrm{K,Ca}}$ following Eq. 21 with $a = 45mV$ and $b = 30mV$. Note that the dynamics is relevant at physiological membrane potentials.

sigmoidal function for the voltage-dependent activation with $V_{\mathrm{K,Ca}} = -40mV$ and $\kappa_{\mathrm{K,Ca}} = 25mV$. We then get the result shown in Figure 13. A physiological interpretation of Eq. 21 is not obvious. Basically this equation says that less calcium is needed to reach the same level of activation when the cell is more depolarised. If the dependence of the opening probability

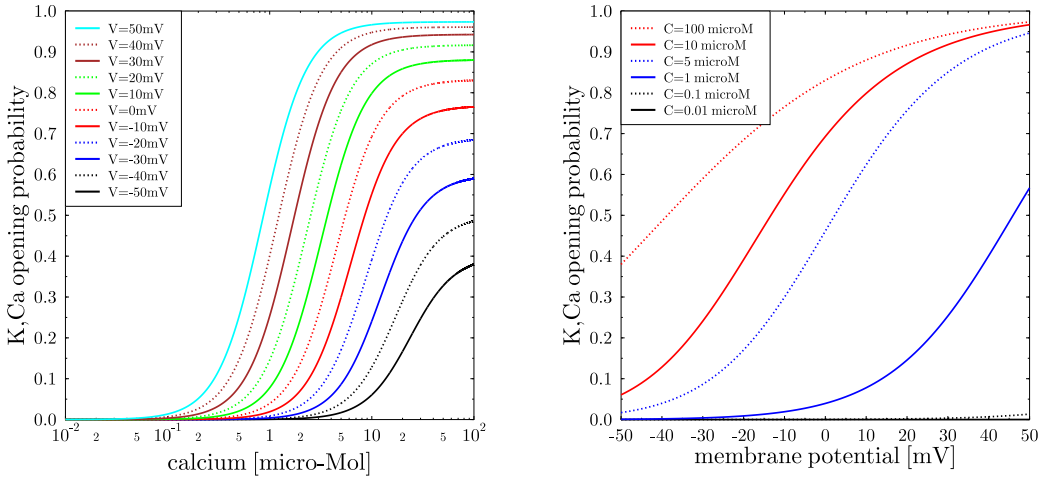

Figure 13: Opening probability of K,Ca using a product of a sigmoidal function (for V) and a Hill-function (for calcium). The calcium concentration of half activation is assumed to depend on the membrane potential according to Eq. 21. The results are shown varying calcium (left panel) or the membrane potential (right panel). There is good agreement with the data in Fig. 8 (14). Parameters are $a = 45mV$, $b = 30mV$, $n_{\mathrm{K,Ca}} = 2$, $V_{\mathrm{K,Ca}} = -40mV$, and $\kappa_{\mathrm{K,Ca}} = 25mV$.

on voltage and calcium level are supposed to correspond to two different molecular gating-mechanisms, then this equation says that either depolarisation acts on both mechanisms or the mechanism influenced by depolarisation acts back on the calcium-dependent mechanism. A concise interpretation is, however, lacking, and has to be clarified in further experiments.

Inactivation: Inactivation was only rarely observed. In rat muscle cells the channels remained open for several hundred milliseconds (14). Thus, inactivation of these channels is neglected in the model.

5.1.8 Small conductance calcium-gated potassium channel sK,Ca

In addition to the potassium channel K,Ca described in Section 5.1.7 a small conductance variant of a calcium-gated potassium channel is expressed in pancreatic β-cells (38, 42). The small conductance version is denoted by sK,Ca and is modelled as

$$I_{\mathrm{sK,Ca}} \;=\; g_{\mathrm{sK,Ca}}\, \overline{g_{\mathrm{sK,Ca}}}\, \left(V - \overline{V_{\mathrm{K}}}\right) \tag{22}$$

with

$$\frac{dg_{\mathrm{sK,Ca}}}{dt} \;=\; \frac{\sigma_{\mathrm{act}}\left(C, C_{\mathrm{sK,Ca}}, \kappa_{\mathrm{sK,Ca}}\right) - g_{\mathrm{sK,Ca}}}{\tau_{\mathrm{sK,Ca}}} \quad . \tag{23}$$

Channel opening is mainly determined by calcium levels (30), while the membrane potential was not reported to have impact.

Conductance: The sK,Ca-channel is characterised by a low single channel conductance of $\overline{g_{\mathrm{sK,Ca}}} = 0.5pS$ (63). At physiological ionic gradients $0.1pS$ were found.

Activation and inactivation time scales: Activation of the channel happened with a time constant of $2.3s$. Deactivation after stop of stimulation was exponential with $6.5s$ (30). Deactivation shall not be confused with inactivation here, because the channel is not known to inactivate during calcium levels being high. These time scales include the time of rising and decreasing calcium levels, thus, overestimate the real time scale of sK,Ca-activation. The exact activation time scale is taken from corresponding measurements and modelling work $\tau_{\mathrm{sK,Ca}} \approx 75ms$ (64). Note that the observed increased duration of opening for supra-large calcium concentrations is neglected here. Because activation is relatively slow, the channel activity cannot be modelled in the limit of steady state, which gives rise to Eq. 23.

Calcium-dependent opening dynamics: The steepness of activation and half activation calcium can be estimated on the basis of the observation that at physiological calcium the current is only 20% of its maximum (63). It reaches 90% of the possible current after stimulation (30). At the end of a burst the calcium level is about 10-20-fold. Thus

$$\begin{aligned} & \sigma_{\mathrm{act}}\left(C_0, C_{\mathrm{sK,Ca}}, \kappa_{\mathrm{sK,Ca}}\right) = 0.2 \quad \text{and} \quad \sigma_{\mathrm{act}}\left(15C_0, C_{\mathrm{sK,Ca}}, \kappa_{\mathrm{sK,Ca}}\right) = 0.9 \\ \Longrightarrow \quad & C_{\mathrm{sK,Ca}} \approx 0.64\mu M \quad \text{and} \quad \kappa_{\mathrm{sK,Ca}} \approx 0.39\,\mu M \quad . \end{aligned} \tag{24}$$

These values are consistent with the activation curve found in (64) (Figure 1, therein) in xenopus oocytes, where a Hill equation with half value of $0.74\mu M$ was used.

5.1.9 Voltage-gated calcium channels Ca,L/T

Voltage-gated calcium channels induce the inflow of calcium, following the electrochemical gradient of calcium, after an initial depolarisation of the cell. There are different subtypes of these channels which differ in their responsiveness. The dominant types in β-cells resemble L- and T-type channels (27) which can be classified as HVA- and LVA-channels, respectively. The equations for these channels are in analogy to the voltage-gated sodium channels Eq. 9

$$I_{\mathrm{Ca,L}} = h_{\mathrm{Ca,L}}\left(1 - H(C, C_{\mathrm{Ca,L}}, n_{\mathrm{Ca,L}})\right) g_{\mathrm{Ca,L}} \overline{g_{\mathrm{Ca,L}}} \left(V - \overline{V_{\mathrm{Ca}}}\right) \quad , \tag{25}$$

with

$$\begin{aligned} \frac{dg_{\mathrm{Ca,L}}}{dt} &= \frac{\sigma_{\mathrm{act}}(V, V_{\mathrm{Ca,L}}, \kappa_{\mathrm{Ca,L}}) - g_{\mathrm{Ca,L}}}{\tau_{\mathrm{Ca,L}}} \\ \frac{dh_{\mathrm{Ca,L}}}{dt} &= \frac{\sigma_{\mathrm{inact}}(V, W_{\mathrm{Ca,L}}, \lambda_{\mathrm{Ca,L}}) - h_{\mathrm{Ca,L}}}{\theta_{\mathrm{Ca,L}}} \quad . \end{aligned} \tag{26}$$

For T-type channels all L's in the subscript have to be replaced by T. The term $1 - H(\ldots)$ appears only for L-type channels and has to be replaced by 1 for T-type. While HVA-channels were included in different ways in other models, LVA-channels were neglected in all other

models. In the following a set of experiments providing opening characteristics of L- and T-type channels are summarised. The simulations will rely on the single protein characteristics as provided in (18).

Single T-type (LVA) channel properties: Open T-type channels show a single protein conductance of $\overline{g_{\mathrm{Ca,T}}} \approx 10pS$ (18) (measured in dendrites of pyramidal neurons in CA1 hippocampus). They open already for membrane potentials near resting potential in the range of -70 to $-30mV$ with a half opening at $-55mV$ (27). The threshold for opening was also measured in adrenal medulla endothelial cells (in whole-cell patch-mode) to be $-50mV$ with $V_{\mathrm{Ca,T}} = -30mV$ (65) (this experiment uses calcium and not barium). The threshold value of $-50mV$ was also found in (18) with $V_{\mathrm{Ca,T}} = -32mV$. This consistently infers $\kappa_{\mathrm{Ca,T}} \approx 10mV$ in order to find low activity at the activation threshold. Indeed, $\kappa_{\mathrm{Ca,T}} = 7.0mV$ was found in (18). For inactivation $W_{\mathrm{Ca,T}} = -67mV$ and $\lambda_{\mathrm{Ca,T}} = 6.5mV$ are reported in (18). Activation happens on a time scale of $\tau_{\mathrm{Ca,T}} = 10ms$ while inactivation is rapid (27) but is slower with $\theta_{\mathrm{Ca,T}} = 18ms$ (65).

Single L-type (HVA) channel activation: Open L-type channels show a single protein conductance of $\overline{g_{\mathrm{Ca,L}}} \approx 27pS$ (18), measured in dendrites of pyramidal neurons in CA1 hippocampus. In β-cells a single-channel conductance of $22pS$ was found (35). Activation is fast: $\tau_{\mathrm{Ca,L}} = 6ms$ (18). Activation is found between -40 and 0mV ((27), (65) in a whole-endothelial cell measurement, and (34) in whole-cell measurements of mouse β-cells). The activation threshold is higher $-20mV$ in CA1-pyramidal cells (18). The half maximal activation potential is $V_{\mathrm{Ca,L}} = -18mV$ (65) with a width of $\kappa_{\mathrm{Ca,L}} \approx 10mV$. In CA1-pyramidal neurons measured with barium $V_{\mathrm{Ca,L}} = +9mV$ is found with $\kappa_{\mathrm{Ca,L}} = 6mV$ (18) (however, activation depends on the barium concentration in the patch). Channel characteristics have also been measured in β-cells with $V_{\mathrm{Ca,L}} = -3.8mV$ and $\kappa_{\mathrm{Ca,L}} = 8.4mV$ (35). The variability of whole-cell measurements of the currents is presumably related to different protein densities in different cell types rather that to different single-channel characteristics – see (65) and references in the discussion of L-type channels. Another ambiguity comes from the replacement of calcium by barium for technical reasons, which induces differences in the measured conductance.

Calcium- but not voltage-dependent L-type inactivation: Voltage-dependent inactivation is not observed for L-type ((27), (34) in β-cells, (65) in endothelial cells, and (66) in bovine chromaffin cells (whole-cell measurement), (18) for CA1-pyramidal neurons). Thus, $\theta_{\mathrm{Ca,L}} > 1s$ is used. Note that the half inactivation potential and the steepness are irrelevant under these circumstances. Alternatively one could simply set $h_{\mathrm{Ca,L}} = 1$.

However, there is an experiment showing inactivation of L-type channels in cardiac cells upon increased calcium levels (67), which is also found in β-cells (34). Inactivation was characterised by a Hill-function with Hill-coefficient $n_{\mathrm{Ca,L}} = 1$ (thus suggesting inactivation to be mediated by the binding of calcium ions to a single regulating site per Ca,L-protein) and half maximal inactivation at $C_{\mathrm{Ca,L}} = 4\mu M$. This behaviour is included in this model for the first time by the additional factor $1 - H(C, C_{\mathrm{Ca,L}}, n_{\mathrm{Ca,L}})$ in Eq. 25.

Sodium conductance: In the same paper (35) it is also shown that the L-type calcium channels exhibit large conductance of $44pS$ for sodium, which is not considered in the simulations.

5.2 The leakage currents

The leakage currents in Eqs. 1 and 4 are calculated in the steady state approximation.

$$\begin{aligned}
-J_{\mathrm{Na}} &= \rho_{\mathrm{Na,V}} I^{\mathrm{ss}}_{\mathrm{Na,V}} + 2\rho_{\mathrm{Na,K}} I^{\mathrm{ss}}_{\mathrm{Na,K}} \alpha_{\mathrm{Na,K}} + \rho_{\mathrm{NCX}} I^{\mathrm{ss}}_{\mathrm{NCX}} \alpha_{\mathrm{NCX}} \\
-J_{\mathrm{K}} &= \rho_{\mathrm{K,ATP}} I^{\mathrm{ss}}_{\mathrm{K,ATP}} + \rho_{\mathrm{K,V}} I^{\mathrm{ss}}_{\mathrm{K,V}} + \rho_{\mathrm{sK,Ca}} I^{\mathrm{ss}}_{\mathrm{sK,Ca}} + \rho_{\mathrm{K,Ca}} I^{\mathrm{ss}}_{\mathrm{K,Ca}} - 2\rho_{\mathrm{Na,K}} I^{\mathrm{ss}}_{\mathrm{Na,K}} \\
-J_{\mathrm{Ca}} &= \rho_{\mathrm{Ca,L}} I^{\mathrm{ss}}_{\mathrm{Ca,L}} + \rho_{\mathrm{Ca,T}} I^{\mathrm{ss}}_{\mathrm{Ca,T}} - z_{\mathrm{Ca}} \rho_{\mathrm{NCX}} I^{\mathrm{ss}}_{\mathrm{NCX}} + \rho_{\mathrm{PMCA}} I^{\mathrm{ss}}_{\mathrm{PMCA}} \quad , \qquad (27)
\end{aligned}$$

where the superscript ss denotes the steady state quantities. The calculated leakage currents guarantee that the cell exhibits a stable steady state and that the cell returns to its resting state after stimulation. In most alternative approaches the leakage currents were not considered (e.g. (3–5)).

The steady state currents are calculated from the steady state approximation of all kinetic equations for the open probabilities. These are evaluated on the basis of a set of properties in the resting state $\{V_0, \gamma_0, N_0, K_0, C_0\}$.

$$\begin{aligned}
I^{\mathrm{ss}}_{\mathrm{Na,K}} &= \overline{I_{\mathrm{Na,K}}} \left(1 - H(K_0, K_{\mathrm{Na,K}}, n_{\mathrm{Na,K}})\right) \\
I^{\mathrm{ss}}_{\mathrm{Na,V}} &= \sigma_{\mathrm{act}}(V_0, V_{\mathrm{Na,V}}, \kappa_{\mathrm{Na,V}}) \overline{g_{\mathrm{Na,V}}} \left(V_0 - \overline{V_{\mathrm{Na}}}\right) \\
I^{\mathrm{ss}}_{\mathrm{NCX}} &= \overline{I_{\mathrm{NCX}}} H(C_0, C_{\mathrm{NCX}}, n_{\mathrm{NCX}}) \\
I^{\mathrm{ss}}_{\mathrm{PMCA}} &= \overline{I_{\mathrm{PMCA}}} H(C_0, C_{\mathrm{PMCA}}, n_{\mathrm{PMCA}}) \\
I^{\mathrm{ss}}_{\mathrm{K,ATP}} &= \left(1 - \sigma_{\mathrm{act}}(\gamma_0, \gamma_{\mathrm{K,ATP}}, \kappa_{\mathrm{K,ATP}})\right) \overline{g_{\mathrm{K,ATP}}} \left(V_0 - \overline{V_{\mathrm{K}}}\right) \\
I^{\mathrm{ss}}_{\mathrm{K,V}} &= \sigma_{\mathrm{act}}(V_0, V_{\mathrm{K,V}}, \kappa_{\mathrm{K,V}}) \overline{g_{\mathrm{K,V}}} \left(V_0 - \overline{V_{\mathrm{K}}}\right) \\
I^{\mathrm{ss}}_{\mathrm{sK,Ca}} &= \sigma_{\mathrm{act}}(C_0, C_{\mathrm{sK,Ca}}, \kappa_{\mathrm{sK,Ca}}) \overline{g}_{\mathrm{sK,Ca}} \left(V_0 - \overline{V_{\mathrm{K}}}\right) \\
I^{\mathrm{ss}}_{\mathrm{K,Ca}} &= \overline{g}_{\mathrm{K,Ca}} \left(V_0 - \overline{V_{\mathrm{K}}}\right) H(C_0, C_{\mathrm{K,Ca}}(V_0), n_{\mathrm{K,Ca}}) \sigma_{\mathrm{act}}(V_0, V_{\mathrm{K,Ca}}, \kappa_{\mathrm{K,Ca}}) \\
I^{\mathrm{ss}}_{\mathrm{Ca,L}} &= \sigma_{\mathrm{act}}(V_0, V_{\mathrm{Ca,L}}, \kappa_{\mathrm{Ca,L}}) \overline{g_{\mathrm{Ca,L}}} \left(V_0 - \overline{V_{\mathrm{Ca}}}\right) \\
I^{\mathrm{ss}}_{\mathrm{Ca,T}} &= \sigma_{\mathrm{act}}(V_0, V_{\mathrm{Ca,T}}, \kappa_{\mathrm{Ca,T}}) \overline{g_{\mathrm{Ca,T}}} \left(V_0 - \overline{V_{\mathrm{Ca}}}\right) \quad , \qquad (28)
\end{aligned}$$

where $C_{\mathrm{K,Ca}}(V_0)$ is calculated with Eq. 21. The intracellular resting concentrations of ions are given in Tab. 2: $K_0 = 95mM$ (68), $N_0 = 20mM$ (68), $C_0 = 0.1\mu M$.

5.3 Additional figures

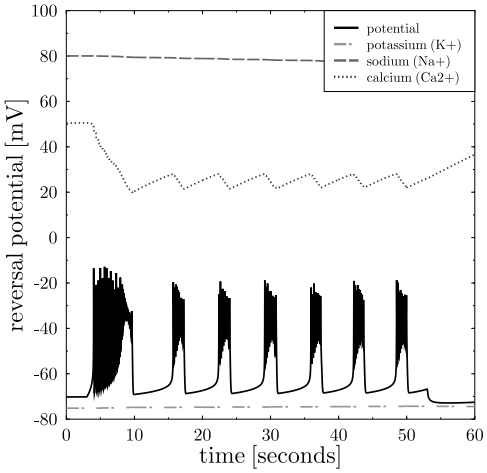

Figure 14: **The dynamics of the reversal potential:** The time course of the reversal potential and the membrane potential (black full line) are depicted. The calcium curve clearly exhibits changes of the reversal potential during a burst. These dynamics influence the burst duration.

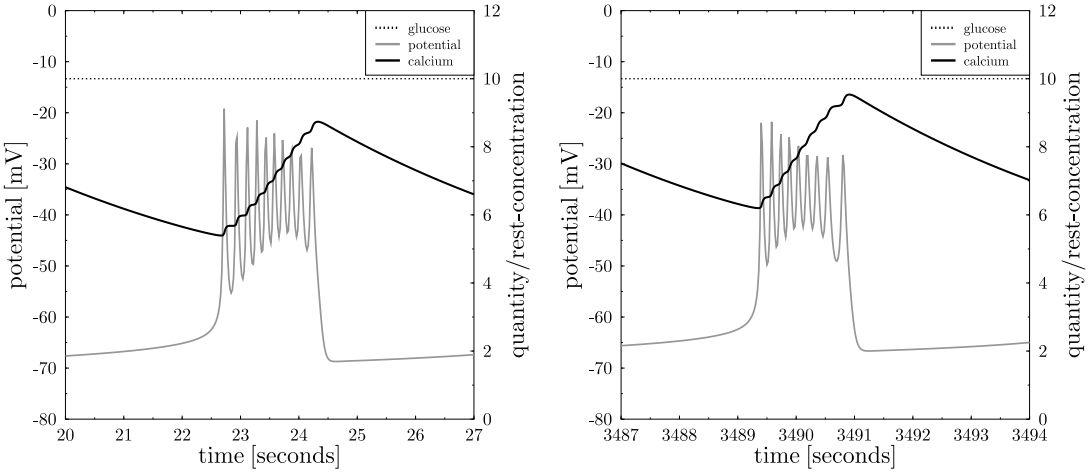

Figure 15: **Comparing bursts during long-term stimulation:** High resolution pictures of bursts at the beginning and at the end of the stimulation period of one hour are compared. At higher sodium level (170% at the end of the glucose stimulation period) the spiking and bursting baselines are slightly elevated, the spiking amplitude is reduced, the duration of the burst is shortened, and the overall calcium level is increased.

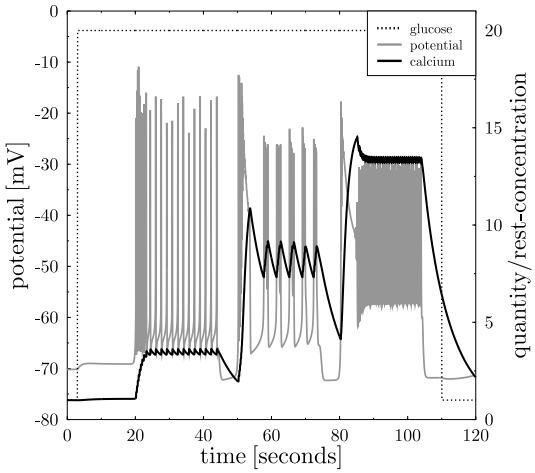

Figure 16: **Simulation with a mutated K,ATP-channel:** A mutated variant of the K,ATP-channel (31) is simulated by increasing the half inhibition glucose concentration $\gamma_{\mathrm{K,ATP}}$ and the width $\kappa_{\mathrm{K,ATP}}$ by a factor of 10. The mutated cell exhibits a steady state. Stimulation with $20mM$ glucose at $t = 3s$ induces only a tiny increase of the resting potential. Then K,ATP is blocked in three steps to 50, 40, and 30% at $t = 20, 50, 80s$, respectively. This induces fast spiking, bursting, and continuous spiking, respectively. The restoration of electrical activity in the mutated variant of the K,ATP-channel by tolbutamide-block was also found in experiment (31).

5.4 Parameter lists

Variable	model Figure 2	full model Figure 3	unit	reference
use leakage currents	no	yes	boolean	–
use inactivation	yes	yes	boolean	–
PMCA feedback to V	no	yes	boolean	–
cell radius R_{cell}	6.1	6.1	μm	(69, 70)
C_{m}	10	10	$fF/\mu m^2$	(71, 72)
T	310	310	K	–
γ_0	1	1	mM	(62)
$\gamma_{\mathrm{stimualtion}}$	none	10	mM	(28, 72)
V_0	-70	-70	mV	known
K_0	95	95	mM	(68)
K_{ext}	5.7	5.7	mM	Eq. 5: $\overline{V_{\mathrm{K}}} = -75mV$
N_0	20	20	mM	(68): 20, (73): 36
N_{ext}	400	400	mM	Eq. 5: $\overline{V_{\mathrm{Na}}} = 80mV$
C_0	0.1	0.1	μM	known
C_{ext}	1.5	1.5	mM	Eq. 5: $\overline{V_{\mathrm{Ca}}} = 128mV$
use Nernst	no	yes	boolean	–
correct $\overline{V_{\mathrm{Ca}}}$	no	78	mV	(15): $\overline{V_{\mathrm{Ca}}} = 50mV$
calcium binding sites c_0	1.0	1.0	mM	(3): $0.3mM$; 1.0 implies $f_{\mathrm{Ca}} \approx 0.1\%$
K_c	1	1	μM	(74)

Table 2: **General framework of the simulations:** The parameters as used in the full simulation in Figure 3 and the parameters needed to reproduce the model (3) (see Figure 2) are listed. Note that the latter differ from the values used in (3) and are adapted to today's knowledge. References given without comment support the value used in the full model.

Variable	model Figure 2	full model Figure 3	unit	reference
$\overline{I_{\mathrm{Na,K}}}$	none	0.00003	pA	(51)
$K_{\mathrm{Na,K}}$	none	33.3	mM	(49)
$n_{\mathrm{Na,K}}$	none	2	#	(49)
$\tilde{K}_{\mathrm{Na,K}}$	none	20	mM	(49)
$\tilde{n}_{\mathrm{Na,K}}$	none	2	#	(49)
$\alpha_{\mathrm{Na,K}}$	none	1.5	Na/K	known
$\overline{g_{\mathrm{K,ATP}}}$	none	54	pS	(8, 9, 27)
$\tau_{\mathrm{K,ATP}}$	none	1	s	relatively slow
$\gamma_{\mathrm{K,ATP}}$	none	1.2	mM	large current at resting state (7)
$\kappa_{\mathrm{K,ATP}}$	none	6	mM	(26)
$\overline{g_{\mathrm{K,V}}}$	10	10	pS	(27)
$\tau_{\mathrm{K,V}}$	Eq. 18	Eq. 18	s	(29)
half max $\tau_{\mathrm{K,V}}$	0.03	0.03	s	$8ms < \tau_{\mathrm{K,V}} < 37ms$ (29)
$V_{\mathrm{K,V}}$	-15	1.0	mV	(29)
$\kappa_{\mathrm{K,V}}$	5.6	8.5	mV	(29)
$\theta_{\mathrm{K,V}}$	none	400	ms	(29) $\leq 400ms$
$W_{\mathrm{K,V}}$	none	-25	mV	(29)
$\lambda_{\mathrm{K,V}}$	none	7.3	mV	(29)
$\overline{g_{\mathrm{sK,Ca}}}$	none	0.5	pS	(63)
$C_{\mathrm{sK,Ca}}$	none	0.64	μM	(30, 64)
$\kappa_{\mathrm{sK,Ca}}$	none	0.39	μM	(30)
$\tau_{\mathrm{sK,Ca}}$	none	75	ms	(64) Figure 13
$\overline{g_{\mathrm{K,Ca}}}$	220	220	pS	(27), (14): $f(T)$
$C_{\mathrm{K,Ca}}$	0.001	Eq. 21	mM	(14): $f(V)$
$n_{\mathrm{K,Ca}}$	3	2	#	(14)
$\tau_{\mathrm{K,Ca}}$	none	100	ms	estimated
$V_{\mathrm{K,Ca}}$	none	-40	mV	(14)
$\kappa_{\mathrm{K,Ca}}$	none	25	mV	(14)
$\overline{g_{\mathrm{Na,V}}}$	none	14	pS	(52)
$\tau_{\mathrm{Na,V}}$	none	Eq. 11	s	(15, 26)
$V_{\mathrm{Na,V}}$	none	-35	mV	(19)
$\kappa_{\mathrm{Na,V}}$	none	8.0	mV	(19)
$\theta_{\mathrm{Na,V}}$	none	4.6	ms	(15)
$W_{\mathrm{Na,V}}$	none	-109	mV	(19, 26, 27)
$\lambda_{\mathrm{Na,V}}$	none	20	mV	(19, 26, 33)

Table 3: **Properties of single sodium and potassium conducting transmembrane proteins:** Properties of sodium and potassium conducting membrane proteins. References given without comment support the value used in the full model. A comment of the form $f(X)$ denotes that the reference claim a dependence on the variable X.

Variable	model Figure 2	full model Figure 3	unit	reference
$\overline{I_{\mathrm{NCX}}}$	none	-0.5	fA	(53)
C_{NCX}	none	1.8	μM	(10)
n_{NCX}	none	1	#	(12)
α_{NCX}	none	3	Na/Ca	(10)
$\overline{I_{\mathrm{PMCA}}}$	0.01	0.01	fA	(53)
C_{PMCA}	1.8	0.1	μM	(61)
n_{PMCA}	2	2	#	(59)
α_{PMCA}	1	1	Ca/ATP	(58)
$\overline{g_{\mathrm{Ca,L}}}$	27	27	pS	(18, 35)
$\tau_{\mathrm{Ca,L}}$	1	6	ms	(18): fast
$V_{\mathrm{Ca,L}}$	0.0	0.0	mV	(18, 35, 65)
$\kappa_{\mathrm{Ca,L}}$	12	12	mV	(18, 27, 35)
$\theta_{\mathrm{Ca,L}}$	10	10	s	(18): no inact.
$W_{\mathrm{Ca,L}}$	100	100	mV	(18): no inact.
$\lambda_{\mathrm{Ca,L}}$	10	10	mV	(18): no inact.
$C_{\mathrm{Ca,L}}$	none	4	μM	(34, 67)
$n_{\mathrm{Ca,L}}$	none	1	#	(34, 67)
$\overline{g_{\mathrm{Ca,T}}}$	none	10	pS	(18)
$\tau_{\mathrm{Ca,T}}$	none	10	ms	(65)
$V_{\mathrm{Ca,T}}$	none	-30	mV	(18)
$\kappa_{\mathrm{Ca,T}}$	none	7.0	mV	(18)
$\theta_{\mathrm{Ca,T}}$	none	18	ms	(65)
$W_{\mathrm{Ca,T}}$	none	-67	mV	(18)
$\lambda_{\mathrm{Ca,T}}$	none	6.5	mV	(18)

Table 4: **Properties of single calcium conducting transmembrane proteins:** Properties of calcium conducting transmembrane proteins. References given without comment support the value used in the full model.

Variable	model Figure 2	full model Figure 3	unit	reference
$\rho_{\mathrm{K,ATP}}$	none	0.08	$/\mu m^2$	~ 0.3 (islets) (26, 30)
$\rho_{\mathrm{K,V}}$	0.24	4.9	$/\mu m^2$	$1-7$ (isolated) (29)
$\rho_{\mathrm{sK,Ca}}$	none	0.6	$/\mu m^2$	$0.5-1.1$ (isolated) (30, 63)
$\rho_{\mathrm{K,Ca}}$	0.08	0.4	$/\mu m^2$	
$\rho_{\mathrm{Na,K}}$	none	2000	$/\mu m^2$	
$\rho_{\mathrm{Na,V}}$	none	1.4	$/\mu m^2$	~ 1 (isolated) (19, 33)
ρ_{NCX}	none	14	$/\mu m^2$	
ρ_{PMCA}	10000	1100	$/\mu m^2$	
$\rho_{\mathrm{Ca,L}}$	0.1	0.7	$/\mu m^2$	$0.3-0.9$ (isolated) (29, 32–35)
$\rho_{\mathrm{Ca,T}}$	none	0.15	$/\mu m^2$	species-dependent

Table 5: **Densities of ion-conducting transmembrane proteins:** The densities of transmembrane proteins as used in the two simulation set-ups are listed. These parameters were estimated by whole cell conductance data (see references) and used as fit parameters for the simulations. The currents differ strongly between experiments in intact islets and with isolated β-cells (factor $2-7$ less, e.g. (30)), thus, the system is specified and if the relative factor is known it is incorporated into the value. The data stem from mice, rats or humans. Note that the large PMCA-density is a result of an unrealistic half activation calcium concentration used in (3) (see also Tab. 4).